

# The combination of MnO<sub>2</sub>@Lipo-coated gefitinib and bevacizumab inhibits the development of non-small cell lung cancer

Jisong Zhang\*, Li Xu\*, Huihui Hu and Enguo Chen

Department of Pulmonary and Critical Care Medicine, Regional Medical Center for National Institute of Respiratory Diseases, Sir Run Run Shaw Hospital, School of Medicine, Cancer Center, Zhejiang University, Hangzhou, China

## ABSTRACT

It can be found from a large number of cancer treatments that use of anti-cancer drugs alone often presents low efficacy and high side effects. This study aims to develop a new drug carrier with tumor-specific response, controlled release *in vivo* and high tumor-suppressive property. Inorganic nano-materials MnO<sub>2</sub> with pH and glutathione (GSH, abundant in cancer cells) responsiveness were used to construct sustained-release functional nano-liposome to be an excellent *in vivo* pH-sensitive drug delivery system. Some hydrophilic MnO<sub>2</sub>, gefitinib (Geb), and bevacizumab (Beb) were encapsulated in the phospholipid vesicles (liposomes), so as to integrate several anti-tumor drugs (MnO<sub>2</sub>-PDA@Lipo@Geb@Beb) to achieve effective treatment of non-small cell lung cancer (NSCLC). Part of the MnO<sub>2</sub> nanorods on the lipid shell had the properties of pH and GSH responsiveness, which could further enhance anti-cancer efficacy. Cell assay results showed that MnO<sub>2</sub>-PDA@Lipo@Geb@Beb nano-drug had an effective inhibition on A549 cell progression and showed excellent biocompatibility. *In vivo* results further confirmed that MnO<sub>2</sub>-PDA@Lipo@Geb@Beb nano-drug could effectively inhibit the growth of NSCLC cells. Overall, it can be inferred from the above experimental results that the nano-composite drug is expected to be widely used in the clinical application of lung cancer.

## ARTICLE HISTORY

Received 24 August 2021  
Revised 13 January 2022  
Accepted 17 January 2022

## KEYWORDS

Specific response; pH-sensitive; NSCLC; biocompatibility



## 1. Introduction

At present, with the in-depth research of nanotechnology, it is found that new nano-materials with unique and excellent properties are expected to improve the clinical medical level in essence (Wicki et al., 2015; Selvakumar et al., 2016). Especially, the cancer-specific drug nanocarriers can largely overcome the tumor heterogeneity, angiogenesis, complex microenvironment, and other factors, which accumulate within the cancer tissue through enhanced permeability and retention (EPR) effect, thereby improving the inhibition of cancer by traditional drug therapy without affecting the other normal cells around the cancer (Maeda et al., 2000; Jin et al., 2018; Prasad et al., 2018; Wu et al., 2018). Most importantly, characteristics of chemicals such as hydrogen ions (H<sup>+</sup>), glutathione (GSH), hydrogen peroxide (H<sub>2</sub>O<sub>2</sub>), and oxygen (O<sub>2</sub>) in cancer cells increase dangers of cancer (Lusic & Grinstaff, 2013; Alizadeh et al., 2015; Prasad et al., 2019). Therefore, application of a nano-drug carrier that simultaneously responds to and regulates the tumor microenvironment is the best way to treat malignant tumor.

The research on nano-drug carriers is very extensive, usually involving polymers, lipids, proteins, inorganic materials, and other composites (Zhang et al., 2007; Lohcharoenkal

et al., 2014; Han et al., 2016; Chen et al., 2018). Due to good biocompatibility, biodegradability, and low toxicity, nano-liposomes have been widely used in biomedical fields, such as vaccine delivery, drug carrier, and gene therapy (Allen & Cullis, 2013; Ying et al., 2016; Chen et al., 2017). Liposomes are hydrophilic spherical vesicles composed of phospholipid bilayers and its unique structure can coat many water-soluble drugs (Zamboni, 2005; Zununi Vahed et al., 2017). In this way, the tissue distribution and plasma clearance (CL) of the coated drugs *in vivo* can be changed, and the pharmacokinetic characteristics specific to drug nano-liposome carriers are given (Papahadjopoulos et al., 1991; Lasic et al., 1992; Drummond et al., 1999; Barenholz, 2003). However, the nano-liposome itself does not have active specific accumulation in cancer sites. Hence, it is necessary to design new nano-liposome composite materials. Some specific nano-materials are used to modify the liposomes so that liposomes can rapidly reach the cancer site and accumulate for a long time after intravenous injection, thus improving the therapeutic effect of anti-cancer drugs on cancer.

At present, most studies on the modification of nano-liposomes use some organic polymer materials with tumor specificity, such as polymers, polypeptides, and protein antibodies to form active targeting composite specific liposomes,

**CONTACT** Enguo Chen  3195024@zju.edu.cn  Department of Pulmonary and Critical Care Medicine, Regional Medical Center for National Institute of Respiratory Diseases, Sir Run Run Shaw Hospital, School of Medicine, Cancer Center, Zhejiang University, 3# East Qingchun Road, Hangzhou 310016, Zhejiang, China

\*Both authors contributed equally to this work.

© 2022 The Author(s). Published by Informa UK Limited, trading as Taylor & Francis Group.

This is an Open Access article distributed under the terms of the Creative Commons Attribution-NonCommercial License (<http://creativecommons.org/licenses/by-nc/4.0/>), which permits unrestricted non-commercial use, distribution, and reproduction in any medium, provided the original work is properly cited.

including immune liposomes, receptor-mediated liposomes, and glycosylated liposomes (Liu et al., 2011, 2019; Yanasarn et al., 2011). However, there are few reports on the modification of nano-liposomes by using specific inorganic nano-materials. Some studies only combine magnetic  $\text{Fe}_3\text{O}_4$ ,  $\text{SiO}_2$ , or graphene oxide (GOF) with nano-liposomes to enhance tumor imaging diagnosis and photodynamic therapy (Liu et al., 2017; Prasad et al., 2019). It has been reported that inorganic nano-hollow sphere  $\text{MnO}_2$  can be used as a biodegradable drug carrier to realize tumor microenvironment-responsive imaging and specific drug release, as well as improve the hypoxic environment of tumor so as to enhance the effect of cancer treatment (Yang et al., 2017). Therefore, inorganic nano-materials  $\text{MnO}_2$  are expected to give nano-liposomes a response to tumor pH microenvironment and improve the effective release of anti-cancer drugs.

On the other hand, it is extremely rare that only one anti-cancer drug is used in clinical treatment. Under certain circumstances, combined treatment with multiple anti-cancer drugs can effectively increase the cure rate of cancer, which aims to integrate the efficacy of several drugs and effectively interrupt the growth and spread of cancer (Liao et al., 2014; Zhu et al., 2018). The antiangiogenic drug bevacizumab (Beb) can inhibit angiogenesis, growth and metastasis of tumor by acting on vascular endothelial growth factor (VEGF) signaling pathway. In the treatment of advanced non-small cell lung cancer (NSCLC), Beb in combination with other drugs can effectively improve the survival rate of patients. Therefore, this study combined Beb with gefitinib (Geb), an anti-cancer drug that inhibits epidermal growth factor receptor (EGFR), to exert their anti-cancer advantages and effectively inhibit the growth of NSCLC.

Based on the characteristics of the tumor microenvironment of NSCLC and the disadvantages of traditional nano-drug carriers, this project intended to design and synthesize a nano-composite liposome (as shown in Scheme 1) coated with pH/GSH responsive  $\text{MnO}_2$  nanorods, Geb and Beb. Good biocompatibility and sustained release ability of liposomes, as well as the microenvironmental response of  $\text{MnO}_2$  nanorods and the mechanism of mediating endocytosis, can be used to realize effective controlled release of drugs (Zhang et al., 2015, 2017; He et al., 2020). Meanwhile,  $\text{MnO}_2$  nanorods were decomposed into  $\text{Mn}^{2+}$  and reactive oxygen species (ROS) by excessive microacids ( $\text{H}_2\text{O}_2$ ) and GSH in the tumor microenvironment. Thus, the hypoxia characteristics of tumor can be alleviated and the therapeutic effect can be improved. Nanoparticles designed in this project can effectively extend the time of drug action, significantly reduce drug dose, reduce toxic and side effects, and drug frequency in the treatment of NSCLC, which is of great significance in the clinical application of NSCLC.

## 2. Materials and methods

### 2.1. Materials

The chemical reagents used in the preparation processes were all analytically pure without subsequent purification treatment. Potassium permanganate ( $\text{KMnO}_4$ , 99.5%) was

purchased from Shanghai Lingfeng Chemical Reagent Co., Ltd. (Shanghai, China). Concentrated hydrochloric acid (HCl, 37%) was purchased from Xilong Scientific Co., Ltd. (Shantou, China). Sodium hydroxide (NaOH, 96%), dopamine hydrochloride ( $\text{C}_8\text{H}_{11}\text{NO}_2\cdot\text{HCl}$ , DA, 98%), 1,2-dioleacyl-sn-glycero-3-phosphoethanolamine ( $\text{C}_{41}\text{H}_{78}\text{NO}_8\text{P}$ , DOPE, 98%), cholesterol ( $\text{C}_{27}\text{H}_{46}\text{O}$ , 99%), and Geb (98%) were obtained from Shanghai Aladdin Bio-Chem Technology Co., Ltd. (Shanghai, China). Stearamide ( $\text{C}_{18}\text{H}_{37}\text{NO}$ , 85%) was acquired from Guangdong Lanbao Biotechnology Co., Ltd. (Guangzhou, China). Beb (98%) was purchased from Shanghai Biochempartner Co., Ltd. (Shanghai, China).

### 2.2. Preparation of $\text{MnO}_2$ nanorods

$\text{MnO}_2$  nanorods were synthesized by solution precipitation method (Qu et al., 2009). First, 200 mL  $\text{MnSO}_4$  (0.1 mol/L) was mixed with 200 mL  $\text{K}_2\text{S}_2\text{O}_8$  (0.1 mol/L). After stirring at room temperature, 100 mL NaOH (1.2 mol/L) was added to the mixture to form dark brown precipitation immediately. Finally, the precipitation was filtered, washed with deionized water and ethanol, and dried at 60 °C for 24 h.

### 2.3. Surface hydrophilic modification of $\text{MnO}_2$ nanorods

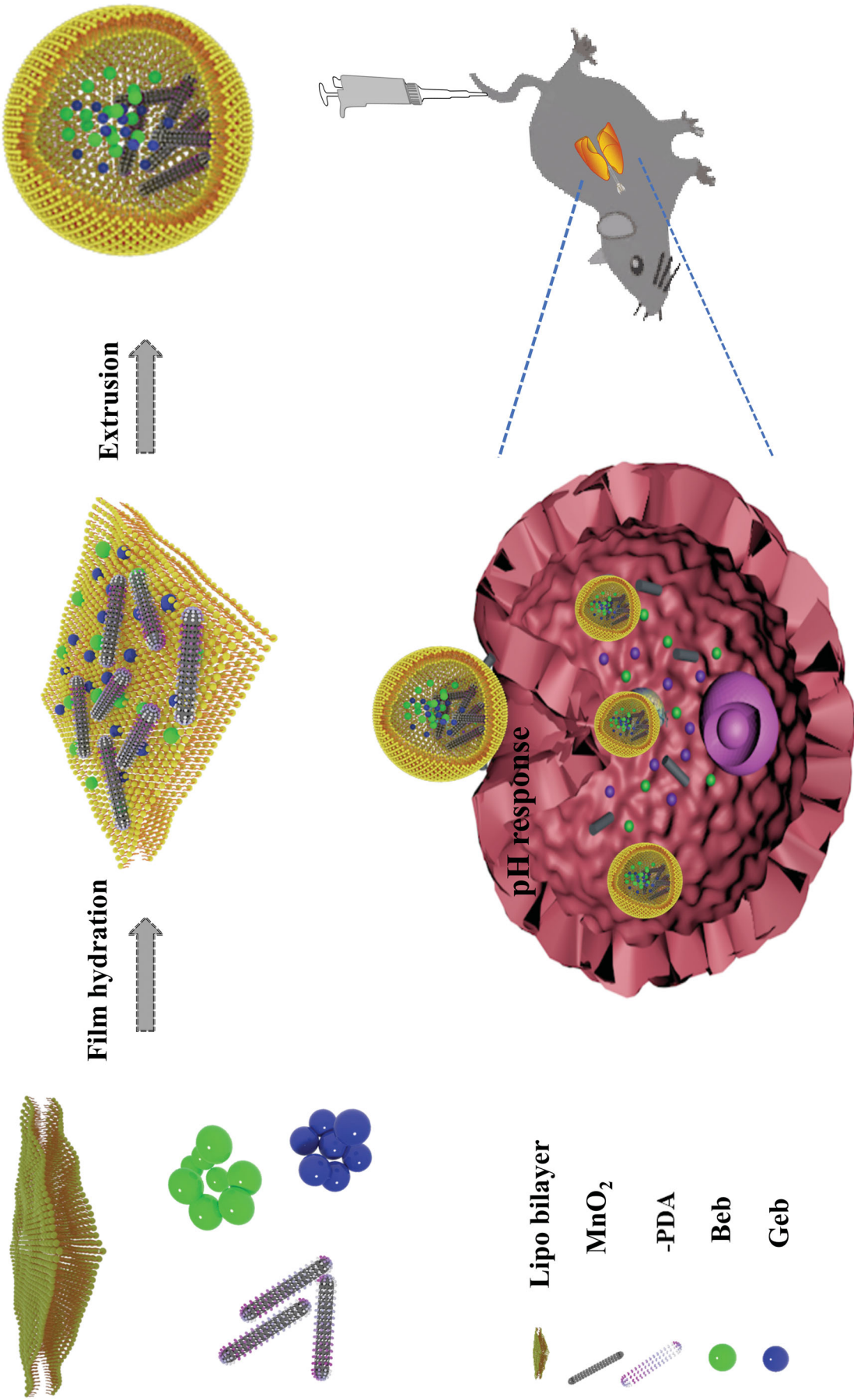
The 0.1 g  $\text{MnO}_2$  particles were uniformly dispersed in 15 mL Tris buffer by ultrasound, and the pH was adjusted to 8.5 by NaOH solution. Then, 0.0013 g DA was added to the suspension and stirred at room temperature for 4 h. The modified  $\text{MnO}_2$  powder was centrifuged and washed with deionized water and anhydrous ethanol. At last, it was dried in a 37 °C oven.

### 2.4. Preparation of $\text{MnO}_2$ -PDA@Lipo@Geb@Beb composite

Cationic liposomes were prepared by using thin-film hydration method to encapsulate anti-cancer drugs Geb and Beb. Cholesterol (5.56 mg), DOPE (44.44 mg), stearamide (5 mg), and Geb (5 mg) were dissolved in chloroform. The solution was ultrasonic at 15 °C. Then, it was transferred to a rotary evaporator for evaporation under a reduced pressure at 40 °C. After film formation, 5 mL  $\text{MnO}_2$ -PDA anhydrous ethanol suspension (0.4 mg/mL) and 200  $\mu\text{L}$  Beb (5 mg) solution were added into the film, followed by ultrasonic for 30 s and worm rotation for 30 min. The liposome membrane vesicles were repeatedly extruded with a 400-nm polycarbonate membrane filter, sealed and stored at low temperature. In addition, the preparation procedures of  $\text{MnO}_2$ -PDA@Lipo@gGeb composite material were the same as above, and Beb was not required in the processes.

### 2.5. Material characterization

The morphology, size, and zeta potential of the samples were characterized by transmission electron microscopy (TEM, JM-2100) and Malvern nano particle size analyzer (Nano-ZS90). The crystal structure of the samples was detected on the X-ray diffractometer (XRD, ARL XTRA;



Scheme 1. Schematic diagram of MnO<sub>2</sub>-PDA@Lipo@Geb@Beb nanocomposite preparation and anti-tumor mechanism.

$2\theta = 10\text{--}80^\circ$ ). The absorbance and concentration of nano-drugs were determined by an ultraviolet–visible (UV–vis) spectrophotometer (Shimadzu, Kyoto, Japan; UV-3600) for determination.

## 2.6. Drug encapsulation efficiency

The encapsulation rate was determined by dialysis method (Mura P et al., 2007). One milliliter drug-carrying liposome was put into a dialysis bag with a molecular weight of 14,000, and then the dialysis bag was placed into 50 mL water–ethanol solution (volume ratio: 1:1). The dialysis was shaken on a shaking table with a rotational speed of  $95\text{ r}\cdot\text{min}^{-1}$ . Samples were taken at different time points and the same amount of dialysis media was supplemented until the sample concentration was constant. The total drug concentration minus the final drug concentration dispersed into the medium was used as the drug concentration encapsulated in the liposome to calculate the drug encapsulation rate.

## 2.7. Drug release rate

Geb and Beb release characteristics in the nanocomposite system were determined by dialysis method. *In vitro* release processes were as follows: first, 5 mL  $\text{MnO}_2\text{-PDA@Lipo@Geb@Beb}$  nanocomposite drug solution was sealed into a dialysis bag (MW: 14,000). After that, it was immersed in 50 mL PBS buffer solution (pH = 5.0, 7.4), and dialysis experiment was conducted at  $37^\circ\text{C}$  under stirring. In the same way, it was immersed in 50 mL buffer solution (pH = 5.0) with or without 10 mM GSH. At each specified time point, 1 mL dialysate was taken out for preservation, and equal amount of fresh PBS solution was added. Finally, the drug release concentrations for Geb and Beb were measured by a UV–vis photometer ( $\lambda = 330\text{ nm}$  or  $272\text{ nm}$ ), and the drug release rate was calculated as follows:

$$\text{Release rate (\%)} = \frac{m_{\text{Releasing}}}{m_{\text{Loading}}} \times 100\% \quad (1)$$

## 2.8. Cell experiments

### 2.8.1. Cell culture

In this study, human NSCLC cell line A549 and human bronchial epithelioid cell line 16HBE cell lines purchased from Shanghai Beinuo Biology Co., Ltd. (Shanghai, China), were used for subsequent cell viability determination test. All experimental cells were inoculated on high-glucose Dulbecco's modified Eagle's medium (H-DMEM) containing 10% (v/v) fetal bovine serum (FBS) and then cultured in an incubator at  $37^\circ\text{C}$  with 5%  $\text{CO}_2$ .

### 2.8.2. Cell internalization experiment

To confirm the endocytosis of cells to composite nanomaterials, the uptake of  $\text{MnO}_2\text{-PDA@Lipo@Geb@Beb}$  treated cells was analyzed. A549 cells ( $1 \times 10^4$  cells/mL) were seeded into

24-well plates for adherent growth. Then, FITC-labeled free Geb,  $\text{MnO}_2\text{-PDA@Lipo@Geb}$ , and  $\text{MnO}_2\text{-PDA@Lipo@Geb@Beb}$  nanoparticles (Geb concentration was  $5\text{ }\mu\text{g/mL}$ ) were added respectively and incubated for a period of time. Each well was washed with PBS, fixed with paraformaldehyde, and stained with 4',6-diamidino-2-phenylindole (DAPI, Sigma, St. Louis, MO). The control groups were set with PBS and  $\text{MnO}_2\text{-PDA@Lipo}$ . Finally, the plates were observed under a confocal laser microscope (TCS SP8 X) and the corresponding fluorescence intensity was quantified by Flow Jo 7.6.1 software (three parallel for each well).

### 2.8.3. Cell viability

*MTT assay:* Cell viability in the experimental and control groups was assessed by MTT assay. A549 and 16HBE cells with densities of  $5 \times 10^4$  cells/mL were inoculated in 96-well plates (containing  $100\text{ }\mu\text{L}$  medium/well), and incubated at  $37^\circ\text{C}$  with 5%  $\text{CO}_2$  overnight. Then, the medium was removed and the cells were suspended in fresh mediums (containing free Geb,  $\text{MnO}_2\text{-PDA@Lipo@Geb}$ ,  $\text{MnO}_2\text{-PDA@Lipo@Geb@Beb}$ ), with concentrations of Geb of 0, 1, 5, and  $10\text{ }\mu\text{g/mL}$ , respectively. At the same time, the cells treated by medium alone were set as the control group. After that, the plates with different treatments were incubated at  $37^\circ\text{C}$  with 5%  $\text{CO}_2$  overnight for 24 h. Afterwards,  $20\text{ }\mu\text{L}$  MTT solution ( $5\text{ mg/mL}$ ) was added to each well dropwise and incubated for 4 h. The original medium was removed completely and  $150\text{ }\mu\text{L}$  dimethyl sulfoxide (DMSO) was added. Finally, the OD value at the wavelength of  $450\text{ nm}$  was detected by a microplate reader (Victor X, PerkinElmer, Waltham, MA).

Double calcein-acetoxymethyl ester (AM)/propidium iodide (PI) (Sigma-Aldrich, St. Louis, MO) staining:  $2\text{ mL}$  A549 cells were inoculated in a six-well plate (density of  $5 \times 10^4$  cells/mL) and incubated at  $37^\circ\text{C}$  with 5%  $\text{CO}_2$  for 24 h. The medium was then removed and  $200\text{ }\mu\text{L}$  fresh medium with suspended nanoparticles ( $50\text{ mg/mL}$ ) was added. The cells were incubated for another 6 h. After that, cells were washed with PBS buffer solution and then added with fresh culture medium for further incubation for 24 h. The cells were then treated with a mixture of calcitonin-AM (living cell staining) and PI (dead cell staining) for 10 min. Finally, cells were observed under an inverted fluorescence microscope (NIB610-FL/NIB620-FL) (green fluorescence for living cells, red fluorescence for dead cells).

### 2.8.4. Cell apoptosis

In this study, flow cytometry was used to study the apoptosis characteristics of cells. In other words, A549 cells were inoculated on a six-well plate at a cell density of  $5 \times 10^4$  cells/mL for 24 h. Then,  $\text{MnO}_2\text{-PDA@Lipo}$ , Geb,  $\text{MnO}_2\text{-PDA@Lipo@Geb}$ , and  $\text{MnO}_2\text{-PDA@Lipo@Geb@Beb}$  were added into each well, and the co-culture continued for 24 h. After co-culture, Annexin V-FITC/PI Double-Dye Kit (BestBio, Shanghai, China) was used to detect cell apoptosis in these groups. The test procedures were described as follows: all cells (floating cells and adherent cells) in each group were

collected, rinsed with PBS several times, and then suspended with Annexin V buffer at the corresponding concentration. The cells were incubated at room temperature and in dark for 30 min. Finally, after a few minutes of treatment with an appropriate amount of PI, cell apoptosis was analyzed by flow cytometry (BD FACSVerser, Piscataway, NJ) immediately.

### 2.8.5. Angiogenesis experiment

When cell fusion reached 80%, the medium was replaced with serum-free DMEM medium, and different groups treated with 50  $\mu\text{g}/\text{mL}$  drug (PBS,  $\text{MnO}_2\text{-PDA@Lipo}$ , free Geb, free Beb;  $\text{MnO}_2\text{-PDA@Lipo@Geb@Beb}$ ) for continuous culture. After 24 h, the supernatant was collected. The HUVEC cells ( $2 \times 10^4$  cells/well) were plated into a 96-well plate precoated with 50  $\mu\text{L}$  Matrigel. HUVEC cells were cultured in conditioned medium (collected serum-free supernatant of A549 cells). Images were taken after incubation for 4 h.

### 2.9. In vivo antitumor and systemic toxicity assessment

In this study, all BALB/c nude mice (4–6 weeks, 18–20 g) were purchased from Shanghai SLAC Laboratory Animal Co., Ltd. (Shanghai, China), and all subsequent animal experiments were approved by the Animal Ethics Committee of the company. All the pre-experimental mice were raised under a suitable environment with light, temperature ( $22 \pm 1^\circ\text{C}$ ), and humidity (50–60%) for a period of time, during which feed and drinking water were sufficient. PBS buffer was mixed with A549 cells at a density of  $5 \times 10^6$  cells/mL at a 1:1 ratio, and then was subcutaneously injected into the abdominal side of experimental mice to construct a group of NSCLC mouse models. When tumor volume reached  $50 \text{ mm}^3$ , the mice were randomly divided into four groups ( $n=3$ ). Mouse models were treated by intravenous injection of 100  $\mu\text{L}$  PBS,  $\text{MnO}_2\text{-PDA@Lipo}$ , Geb,  $\text{MnO}_2\text{-PDA@Lipo@Geb@Beb}$  suspension (Geb = 3 mg/kg, 1 d, 4 d, 7 d, 10 d, and 13 d), respectively. Tumor volume and body

weight of mice were weighed every three days. After 20 days of culture, mice from each group were randomly selected, euthanized, and dissected to weigh the tumor.

On the other hand, in order to detect the systemic toxicity of nano-drugs, mice treated with PBS,  $\text{MnO}_2\text{-PDA@Lipo}$ , Geb,  $\text{MnO}_2\text{-PDA@Lipo@Geb@Beb}$  and cultured for 20 days were also euthanized. The main organs and tumor sites of the mice were then removed, fixed with 4% paraformaldehyde for 48 h. Subsequently, the main organs and tumor sites were paraffin-embedded and sectioned (approximately 5  $\mu\text{m}$ ). When histological observation was performed, tissue sections were stained in advance with hematoxylin and eosin (H&E), and finally the tissue structure of the organs and tumor sections was observed under an optical microscope (Leica, Wetzlar, Germany).

## 3. Results and discussion

### 3.1. Material characterization

The pH/GSH-responsive  $\text{MnO}_2\text{-PDA@Lipo@Geb@Beb}$  nano-composite drug with biocompatibility was prepared according to the preparation scheme in Figure 1. Prior to the synthesis of the composite drug, the hydrothermal method reported in previous study (Ghosh et al., 2017) was first improved to generate structured  $\text{MnO}_2$  nanorods with  $\text{KMnO}_4$  hydrolyzed under acidic conditions and HCl as the structure-directing agent. The chemical reaction could be described as follows:  $2\text{KMnO}_4 + 8\text{HCl} \rightarrow 2\text{KCl} + 2\text{MnO}_2 + 3\text{Cl}_2 + 4\text{H}_2\text{O}$ . As shown in Figure 1(a), it could be observed from TEM image that  $\text{MnO}_2$  nanorods presented a good rod-like structure in relatively uniform size, with the average length and diameter of about 100 nm and 5 nm, respectively. At the same time, in order to improve the hydrophilic property of  $\text{MnO}_2$  nanorods and facilitate their effective compound with nano-liposome drug carriers, this study utilized the oxidative autopolymerization property of DA under alkaline conditions (Zhang et al., 2018) to deposit

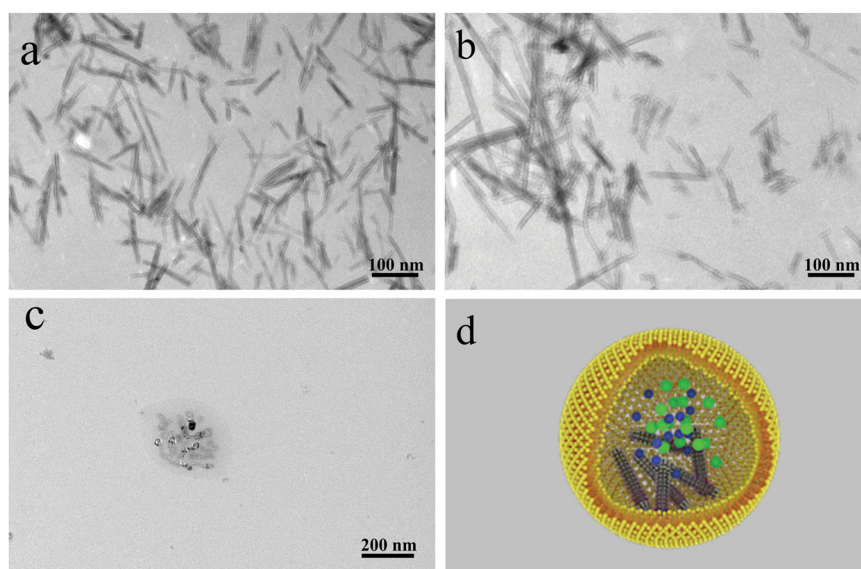


**Figure 1.** (a–c) TEM images of  $\text{MnO}_2$ ,  $\text{MnO}_2\text{-PDA}$ , and  $\text{MnO}_2\text{-PDA@Lipo@Geb@Beb}$  nano-material; (d) structure diagram of  $\text{MnO}_2\text{-PDA@Lipo@Geb@Beb}$ .

a hydrophilic polydopamine (PDA) nano-film on  $\text{MnO}_2$  nanorods. TEM analysis in Figure 1(b) displayed that  $\text{MnO}_2$  nanorods still maintained a complete rod-like structure, and modification of the PDA nano-film did not change basic morphology of  $\text{MnO}_2$  nanorods.

The  $\text{MnO}_2$ -PDA@Lipo@Geb@Beb nanocomposite system was combined with common liposome film hydration method, ultrasound, vortex, and extrusion treatment to finally obtain the required nano-liposome composite structure. In other words,  $\text{MnO}_2$ -PDA, Geb, and Beb were loaded or coated on the surface or in the inner cavity of the phospholipid bilayers by the nano-liposomes formed by the self-assembly of lipids such as cholesterol, DOPE and stearamide. The structure of the prepared material was confirmed by TEM characterization. It could be clearly noted from Figure 1(c) that overall morphology of this composite material presented a complete ellipsoid shape, with the diameter distribution of about 100–200 nm. This confirmed the nano-composite structure we envisaged (Figure 1(d)). In other words, the formed nano-liposomes-coated  $\text{MnO}_2$  nanorods, Geb, and Beb with different anti-cancer mechanisms in the inner cavity of the phospholipid bilayers. The pH/GSH-responsive  $\text{MnO}_2$  nanoparticles were loaded on the interior of the liposomes, so as to realize the accurate and effective release of anti-cancer components in the cancer sites.

The effects of different sintering temperatures and lipid layers on the crystal morphology and characteristic peak strength of the materials were investigated. The crystal

structure of  $\text{MnO}_2$  (400 °C and 600 °C) and  $\text{MnO}_2$ -PDA@Lipo@Geb@Beb nanocomposites after heat treatment at different temperatures was analyzed by typical XRD (Figure 2(a)). According to the statistics in the figure, the diffraction peaks of  $\alpha$ - $\text{MnO}_2$  crystal type (JCPDF-44-0141) (Li et al., 2006) appeared at  $2\theta = 28.82^\circ$ ,  $37.57^\circ$ ,  $42.96^\circ$ ,  $49.95^\circ$ ,  $56.77^\circ$ ,  $60.36^\circ$ ,  $65.18^\circ$ , and  $69.36^\circ$ , which corresponded to (310), (211), (301), (411), (600), (521), (002), and (741) crystal surfaces in turn. The characteristic peaks in the spectrum were relatively sharp without other complex peaks, indicating that the purity of prepared  $\text{MnO}_2$  was very high, and its crystal structure was not changed by heat treatment temperature. On the other hand, it could also be observed that the XRD characteristic peaks of  $\text{MnO}_2$ -PDA@Lipo@Geb@Beb nanocomposite were basically consistent with those of  $\text{MnO}_2$  nanorods. However, compared with  $\text{MnO}_2$  nanorods, the strength of characteristic peaks of  $\text{MnO}_2$ -PDA@Lipo@Geb@Beb was relatively weak and a few miscellaneous peaks were observed, which may be due to the influence of organic components such as nano-liposomes, Geb, and Beb in the composite material.

In this study, surface zeta potentials of the synthesized  $\text{MnO}_2$  and its composites ( $\text{MnO}_2$ ,  $\text{MnO}_2$ -PDA,  $\text{MnO}_2$ -PDA@Lipo,  $\text{MnO}_2$ -PDA@Lipo@Geb@Beb) were also investigated, and the results are exhibited in Figure 2(b). Zeta potentials of the four kinds of materials were as follows:  $\text{MnO}_2$  ( $\zeta = -29.3$  mV) <  $\text{MnO}_2$ -PDA ( $\zeta = -20.4$  mV) <  $\text{MnO}_2$ -PDA@Lipo ( $\zeta = 17.7$  mV) <  $\text{MnO}_2$ -PDA@Lipo@Geb@Beb

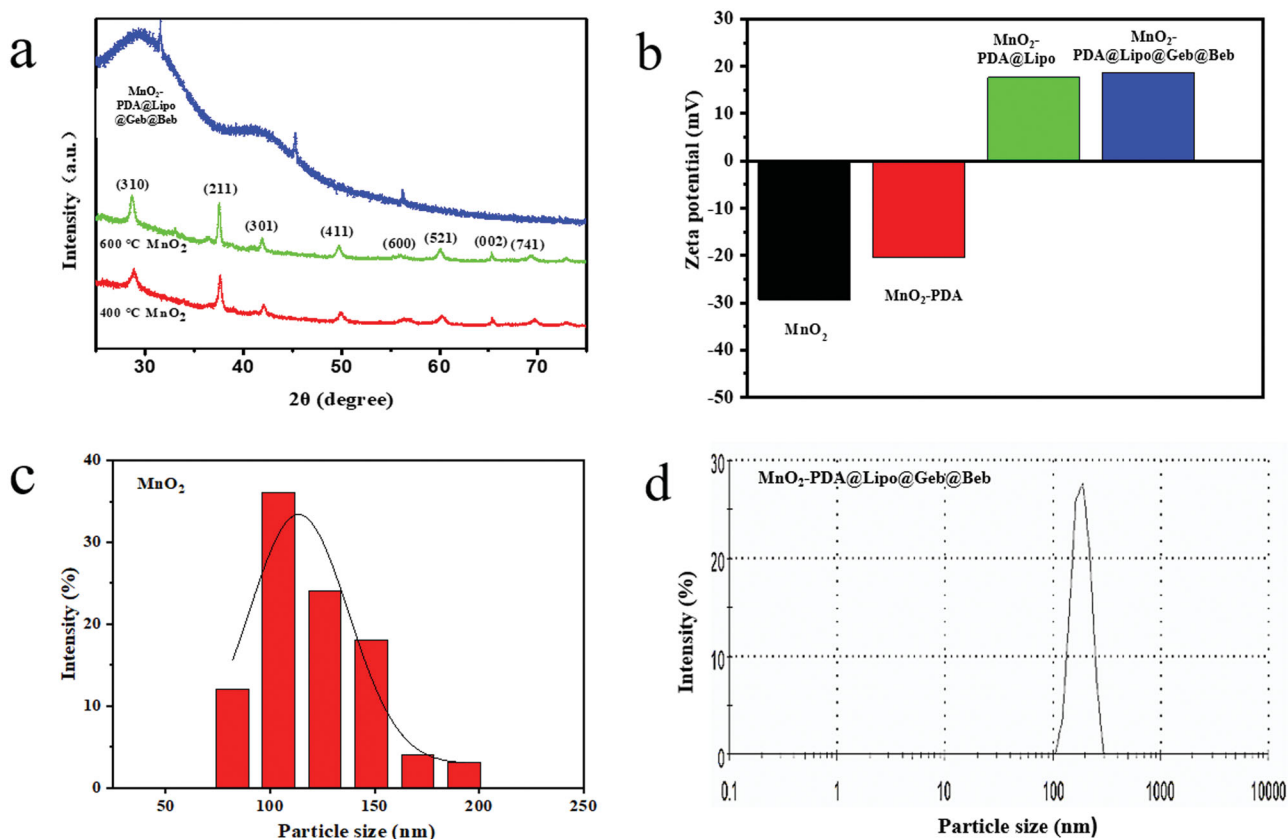


**Figure 2.** (a) XRD patterns of  $\text{MnO}_2$  and its composite after heat treatment at different temperatures; (b) zeta potential; (c) particle size statistical histograms of TEM images of  $\text{MnO}_2$  nanorods; (d) particle distribution of  $\text{MnO}_2$ -PDA@Lipo@Geb@Beb measured by dynamic light scattering (DLS).

( $\zeta = -18.6$  mV). The above results to a certain extent illustrated that cationic liposomes had successfully coated  $\text{MnO}_2$  nanorods and drugs within the phospholipid bilayer cavity ( $\zeta_{\text{MnO}_2} < \zeta_{\text{composites}}$ ). At the same time, the positive surface potential of the composite could generate nonspecific electrostatic adsorption with the negative charge on the surface of cell membrane in the microenvironment of tumor cells.

The particle sizes of  $\text{MnO}_2$  and  $\text{MnO}_2$ -PDA@Lipo@Geb@Beb nano-material were analyzed by particle size analysis software and Malvern nanoparticle size analyzer. Figure 2(c,d) shows their particle size distribution curves. It could be noted from the figure that the particle size of the initial  $\text{MnO}_2$  nanorods was concentrated and distributed at 100 nm. The nano-liposomes were then synthesized by thin-film hydration method, and combined with  $\text{MnO}_2$  nanorods, anticancer drugs by ultrasound, extrusion, and other means. The particle size of the final composite material was concentrated and distributed at about 160 nm.

### 3.2. Study on drug encapsulation and release

To study drug encapsulation efficiency and release characteristics of Geb and Beb, the maximum UV absorption wavelength was determined by UV-vis spectrophotometer at first. Figure 3(a) is the UV-vis absorption spectroscopy of Geb and Beb. It was showed that the maximum absorption wavelengths were  $\lambda_{\text{Geb}} = 330$  nm and  $\lambda_{\text{Beb}} = 272$  nm, respectively. Then, the standard curves of the two drugs were calculated by measuring OD values of drugs at different concentrations. Then, Geb and Beb in the liposomes were completely released by dialysis method. Their absorbance OD values were measured on the UV-vis spectrophotometer, and the drug encapsulation rates of Geb and Beb were determined to be 55.96% and 52.61%, respectively.

Figure 3(b) exhibits the *in vitro* release kinetics curves of Geb and Beb from  $\text{MnO}_2$ -PDA@Lipo@Geb@Beb nano-material in PBS buffer at pH 5.0 and 7.4. It could be observed that Geb and Beb showed a transient and sudden release during 0–6 h with a slow and stable release process in the following 20 h. DOPE is a pH-sensitive phospholipid, and its protonated group makes the end product sensitive and degradable in acidic environment. Then, Geb and Beb will be released gradually with the rupture of liposome membrane. Therefore, compared with pH = 7.4, the cumulative release rates of Geb and Beb were higher when pH = 5.0. After 27 h, the cumulative release rates of both Geb and Beb reached 70% at pH 5.0, which were less than 20% at pH 7.4. In addition, as shown in Figure 3(c),  $\text{MnO}_2$ -PDA@Lipo@Geb@Beb nanomaterials have better drug release performance under high GSH condition compared to non-redox condition, indicating that  $\text{MnO}_2$ -PDA@Lipo@Geb@Beb nanomaterial possesses GSH response characteristic. In fact, the high drug release rate is attributed to the pH response of DOPE as well as the strong reductive response of nano  $\text{MnO}_2$ . As exhibited in Figure 3(d), the  $\text{MnO}_2$  nanorods of this nanomaterial were degraded under acidic and reductive conditions, and the liposome shell was gradually decomposed, in which the  $\text{MnO}_2$ , Geb and Beb drugs were released, thus playing an anticancer role.

### 3.3. Cell viability and apoptosis in vitro

The effects of several synthesized nanodrugs (Geb,  $\text{MnO}_2$ -PDA@Lipo,  $\text{MnO}_2$ -PDA@Lipo@Geb, and  $\text{MnO}_2$ -PDA@Lipo@Geb@Beb) on the viability of A549 and 16HBE cells were evaluated by MTT method, and cells treated with PBS buffer were set as the control group. The results are shown in Figure 4(a,b). With the increase of drug concentration, Geb,  $\text{MnO}_2$ -PDA@Lipo@Geb, and  $\text{MnO}_2$ -

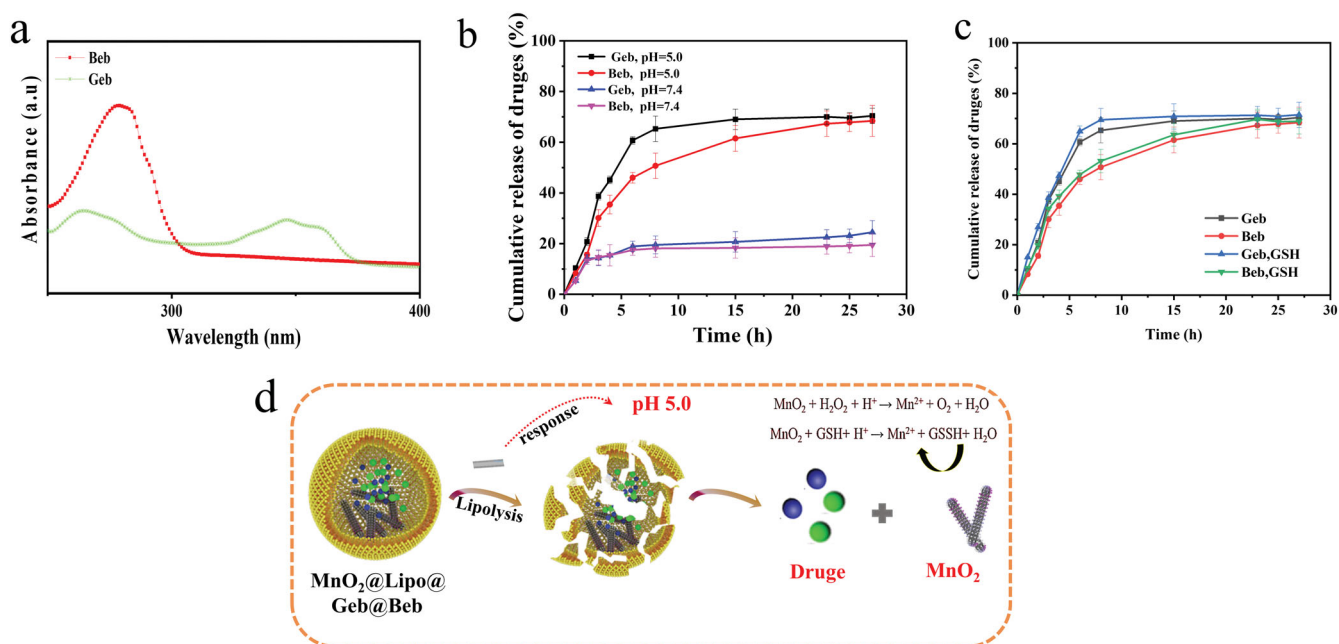


**Figure 3.** (a) UV-vis absorption spectroscopy of Geb and Beb; (b) drug release characteristics of Geb and Beb in  $\text{MnO}_2$ -PDA@Lipo@Geb@Beb composite (pH = 5.0 and 7.4); (c) GSH responsiveness of  $\text{MnO}_2$ -PDA@Lipo@Geb@Beb composite at pH 5.0; (d) drug release mechanism of  $\text{MnO}_2$ -PDA@Lipo@Geb@Beb composite.

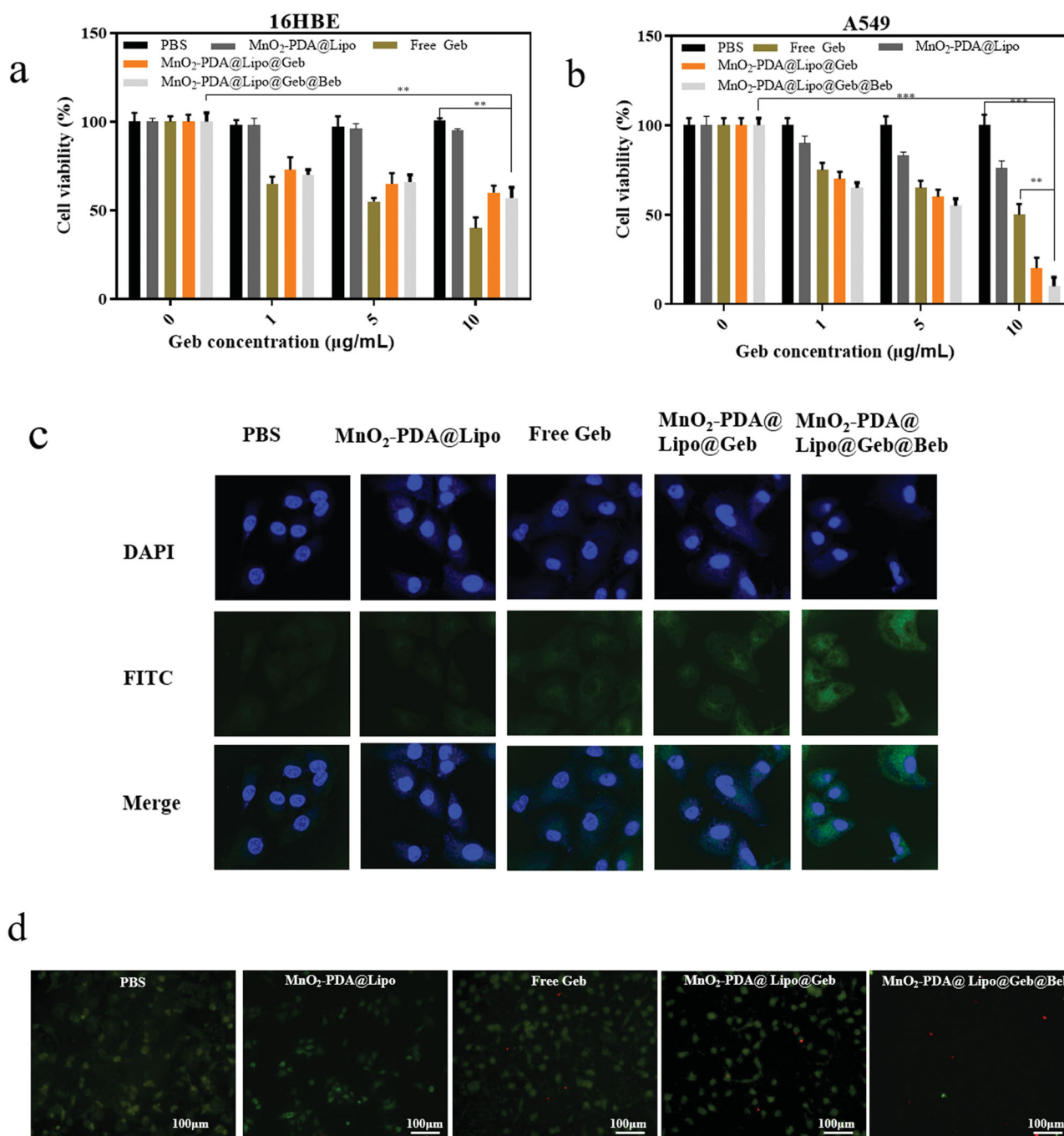


**Figure 4.** (a, b) Cell viability of A549 and 16HBE cells co-cultured with each nano-drug for 24 h (\*\* $p < .01$ , \*\*\* $p < .001$ ); (c) fluorescence imaging of the internalization degree of A549 cells toward various nano drugs; (d) fluorescent pictures of double calcein-AM (green, living cells)/PI (red, dead cells) stained cells.

PDA@Lipo@Geb@Beb all decreased the viability of 16HBE normal bronchial epithelial cells, indicating that they all had certain toxicity to normal cells. Moreover, compared with other materials, Geb alone was more toxic to normal cells, suggesting that the coating of MnO<sub>2</sub>-PDA@Lipo composite material was beneficial to reduce the harmful effect of anti-cancer drugs on normal cells. Meanwhile, Figure 4(b) displays the inhibitory effects of these drugs on A549 cells. The experimental results revealed that the inhibitory ability of these materials on A549 cells all depended on the dose of loaded anti-cancer drugs, and the increase dose of Geb and Beb improved the toxic effect of the materials on lung

cancer cells. Compared with Geb alone, MnO<sub>2</sub>-PDA@Lipo@Geb and MnO<sub>2</sub>-PDA@Lipo@Geb@Beb presented more obvious inhibitory effects on cancer cells. Result of cell internalization (Figure 4(c)) showed that, compared with simple Geb, MnO<sub>2</sub>-PDA@Lipo@Geb, and MnO<sub>2</sub>-PDA@Lipo@Geb@Beb accumulated significantly in A549 cells, and the encapsulation of liposome vesicles was conducive to the accumulation and distribution of drugs in cells.

At the same time, to explore the effect of MnO<sub>2</sub>-PDA@Lipo@Geb@Beb on the proliferation of lung cancer cells, double calcein-AM/PI staining was used for detection (Figure 4(d)). By comparing the number of living cells in the



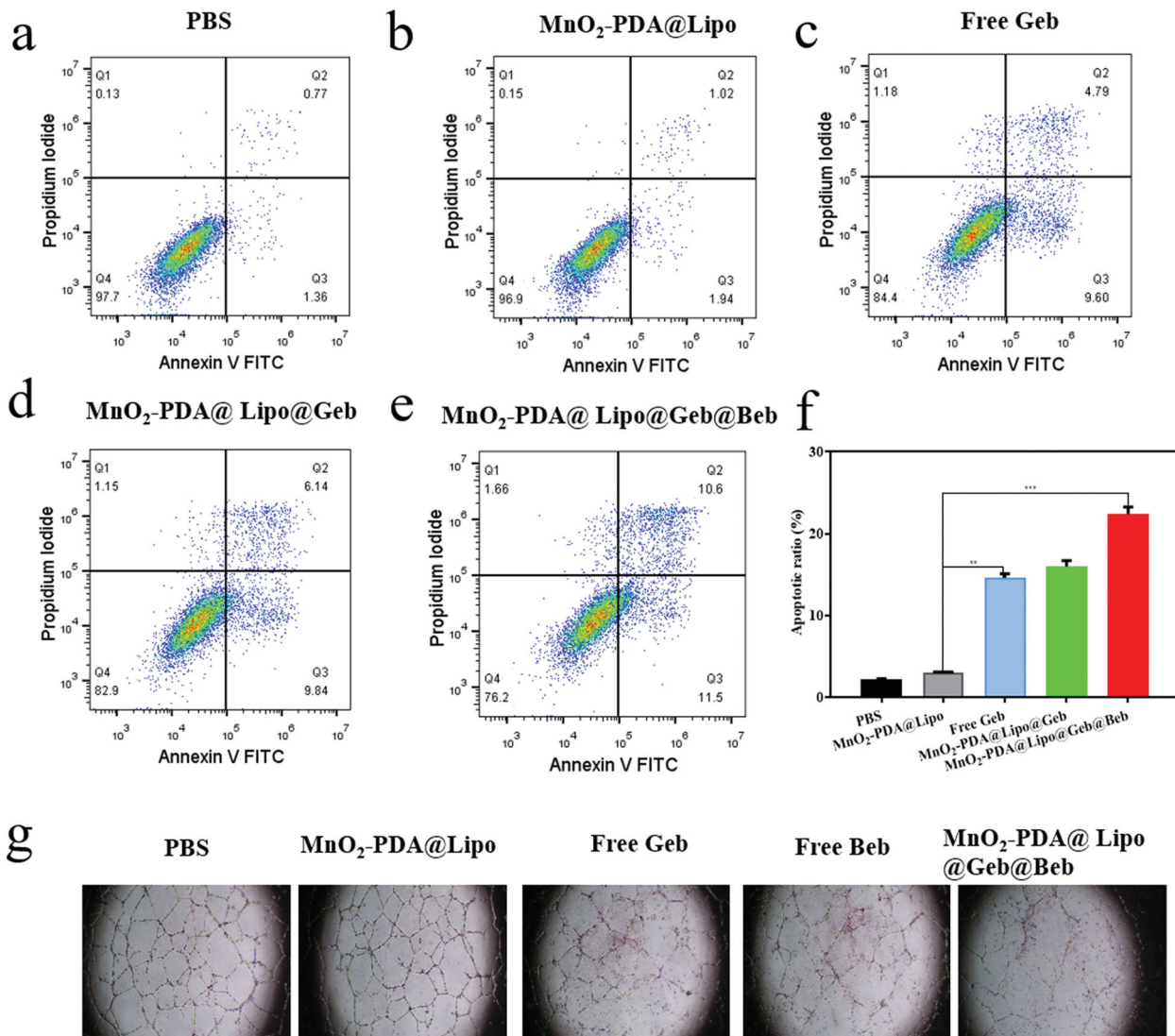


**Figure 5.** (a–e) Flow cytometry and (f) statistical histogram of apoptosis ratio after co-culture of PBS, MnO<sub>2</sub>-PDA@Lipo, Geb, MnO<sub>2</sub>-PDA@Lipo@Geb and MnO<sub>2</sub>-PDA@Lipo@Geb@Beb with A549 cells for 24 h, respectively; (g) the effects of PBS, MnO<sub>2</sub>-PDA@Lipo, free Geb, free Geb; MnO<sub>2</sub>-PDA@Lipo@Geb@Beb treatments on tumor angiogenesis.

fluorescent pictures, more apoptotic A549 cells were found in the MnO<sub>2</sub>-PDA@Lipo@Geb@Beb group. It could be observed that MnO<sub>2</sub>-PDA@Lipo@Geb@Beb inhibited cell proliferation. Flow cytometry was then used for analysis, and the cell apoptosis results are obtained in Figure 5(a–e). Apoptotic data in Figure 5(f) showed that the apoptotic ratio of A549 cells treated with PBS, MnO<sub>2</sub>-PDA@Lipo, Geb, MnO<sub>2</sub>-PDA@Lipo@Geb, and MnO<sub>2</sub>-PDA@Lipo@Geb@Beb was 2.18%, 2.99%, 14.64%, 16.01%, and 22.40%, respectively. Composite drugs coated or loaded with nano-materials were more likely to be internalized by cancer cells and to accumulate in cells in comparison with drugs alone. On the one hand, large number of anti-cancer drugs stored in cells eventually exhibited greater toxicity over time, inducing apoptosis in cancer cells. On the other hand, it was also discovered that the combination of multiple drugs (Geb and Beb) was more effective in inducing apoptosis than the single drug, with a higher apoptotic ratio (22.40%).

The antiangiogenic drug Beb inhibits tumor angiogenesis, growth, and metastasis by acting on the VEGF signaling pathway. In order to further explore the effect of nano-drugs on tumor angiogenesis, MnO<sub>2</sub>-PDA@Lipo, free Geb, free Beb; MnO<sub>2</sub>-PDA@Lipo@Geb@Beb were used to treat A549 cells for subsequent tube formation experiment, and PBS was used as control treatment. Figure 5(g) shows that compared with Geb or Beb treatment alone, MnO<sub>2</sub>-PDA@Lipo@Geb@Beb nanodrug treatment could significantly inhibit tumor angiogenesis and play a greater role in inhibiting tumor growth and metastasis.

### 3.4. In vivo anti-tumor and systemic toxicity assessment

In order to further determine the anti-tumor behavior of MnO<sub>2</sub>-PDA@Lipo, Geb, MnO<sub>2</sub>-PDA@Lipo@Geb, and MnO<sub>2</sub>-PDA@Lipo@Geb@Beb nano-drugs *in vivo*, *in vivo* lung cancer models were established by subcutaneous injection of A549

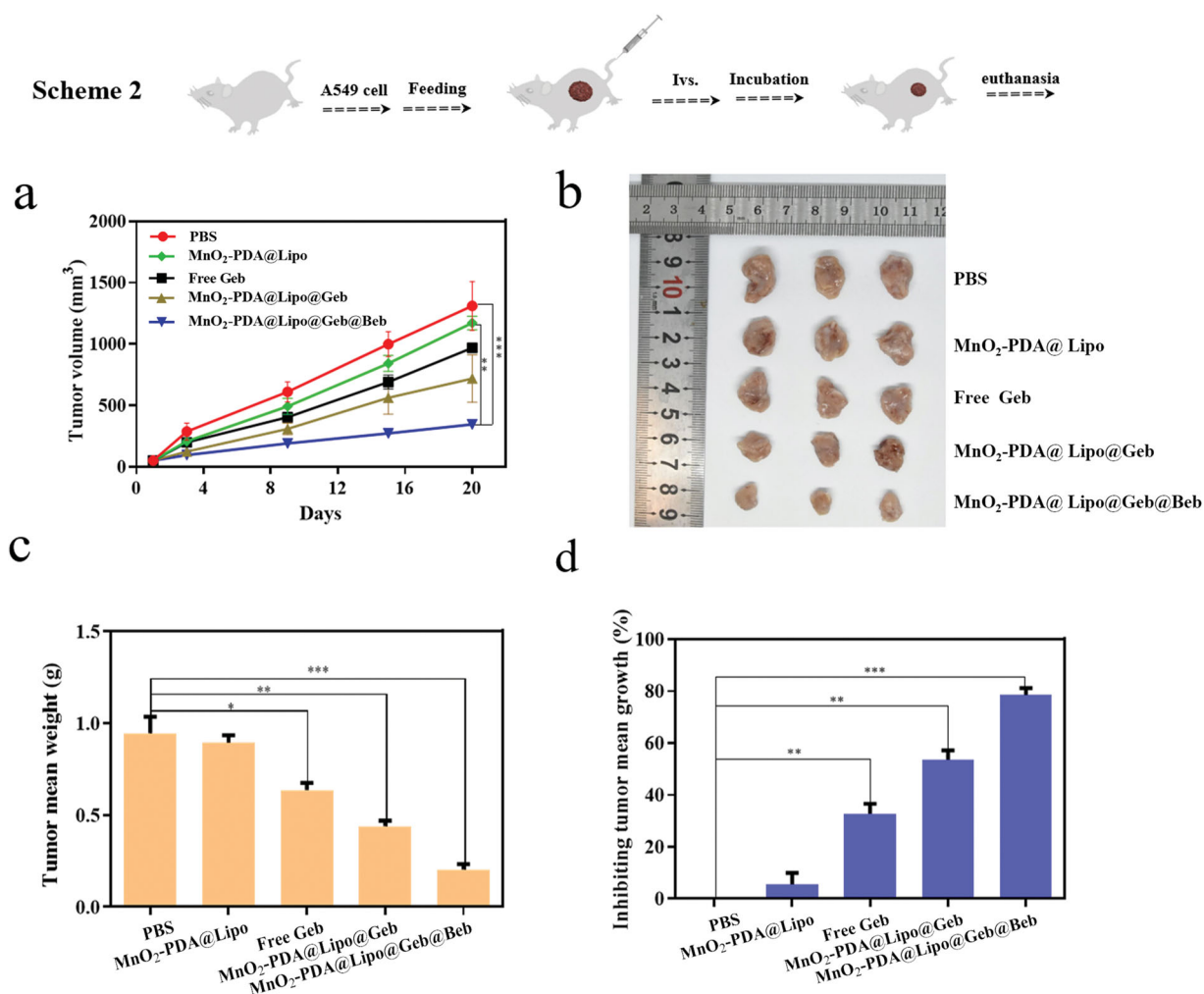


**Figure 6.** Schematic diagram and results of anti-tumor behavior of PBS, MnO<sub>2</sub>-PDA@Lipo, Geb, MnO<sub>2</sub>-PDA@Lipo@Geb, and MnO<sub>2</sub>-PDA@Lipo@Geb@Beb nano-drugs in BALB-c nude mouse tumor models; (a) tumor volume growth trend; (b) tumor therapy renderings; (c) final mean tumor weight after 20 d of treatment; (d) tumor inhibition rate relative to the control group (\* $p < .05$ , \*\* $p < .01$ , \*\*\* $p < .001$ ).

cells into BALB-c nude mice (Scheme 2, Figure 6). In the experiment, mice treated with PBS buffer solution were used as the control group. The anti-cancer activity of several nano-drugs was explored, and the results are in Figure 6. Figure 6(a) manifests that the tumor volume growth trend of MnO<sub>2</sub>-PDA@Lipo@Geb and MnO<sub>2</sub>-PDA@Lipo@Geb@Beb groups slowed down with the extension of treatment time. According to the data in the figure, tumor volume of the MnO<sub>2</sub>-PDA@Lipo @Geb and MnO<sub>2</sub>-PDA@Lipo@Geb@Beb groups decreased by 50.93% and 58.33%, respectively, after 20 d of treatment, compared with that of PBS, MnO<sub>2</sub>-PDA@Lipo, and Geb groups. Simultaneously, the tumor therapeutic effect diagram in Figure 6(b) noted that the anti-cancer drugs coated with MnO<sub>2</sub>-PDA@Lipo had a more significant anti-cancer effect on tumor than free drugs. Besides, the combination of Geb and Beb was more helpful in increasing the lung cancer inhibition rate than using only one anti-cancer drug Geb.

Meanwhile, the final tumor weights were also counted after the experiment (Figure 6(c)). The average tumor weights of the PBS, MnO<sub>2</sub>-PDA@Lipo, Geb, MnO<sub>2</sub>-PDA@Lipo@Geb, and MnO<sub>2</sub>-PDA@Lipo@Geb@Beb groups were 0.946 g, 0.894 g,

0.636 g, 0.439 g, and 0.203 g, respectively, which were consistent with the tumor volume and three-dimensional therapeutic effect diagrams above. At the same time, through further analysis and processing of the experimental data, the tumor inhibition histogram is obtained in Figure 6(d). The inhibition rates of Geb, MnO<sub>2</sub>-PDA@Lipo@Geb, and MnO<sub>2</sub>-PDA@Lipo@Geb@Beb groups were 32.80%, 53.56%, and 78.54%, respectively. The results further confirmed that the anti-tumor activity of Geb was enhanced after it was coated with MnO<sub>2</sub>-modified nano-liposomes, and the combined treatment of MnO<sub>2</sub>-PDA@Lipo@Geb@Beb composite drug showed the best anti-tumor activity.

Similarly, in order to determine whether these synthesized drugs caused systemic toxicity *in vivo*, the drugs were injected intravenously into mice and cultured for 20 d. The heart, liver, spleen, lung, kidney, and tumor sites of mice were removed and observed with H&E staining. From the electron microscope images in Figure 7, except for the simple Geb group, no obvious tissue abnormalities were observed in normal organs of mice in other groups. In the tumor tissue, compared with MnO<sub>2</sub>-PDA@Lipo, GEB, MnO<sub>2</sub>-PDA@Lipo @Geb, the synthesized MnO<sub>2</sub>-

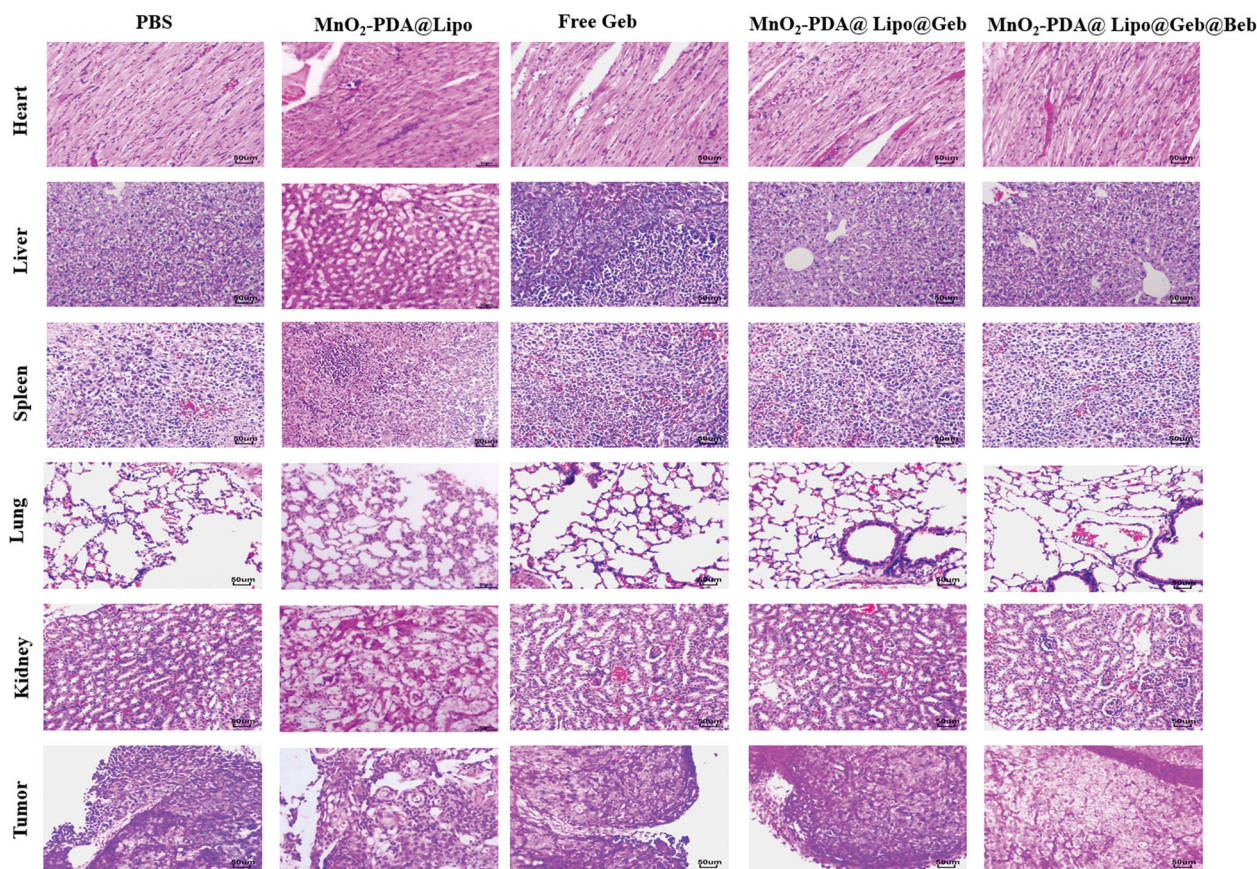


**Figure 7.** Histological study of the whole body of mice: H&E microscopic images of heart, liver, spleen, lung, kidney, and tumor sections (scale: 50  $\mu\text{m}$ ).

PDA@Lipo@Geb@Beb nanocomposite drug could lead to severe necrosis of tumor tissue which further confirmed that MnO<sub>2</sub>-PDA@Lipo@Geb@Beb was superior to Geb alone and single drug-loaded nano-materials in the treatment of lung cancer A549 cells.

To sum up, based on the *in vitro* cell experiments, and analysis of *in vivo* antitumor and systemic toxicity, the nanocomposite drug prepared by Geb and Bed that coated with composite structure of nano liposomes and MnO<sub>2</sub> nanorods had excellent inhibitory effect on A549 cells compared to MnO<sub>2</sub>-PDA@Lipo, Geb, and MnO<sub>2</sub>-PDA@Lipo@Geb drugs, while it showed good biocompatibility to normal cells 16HBE, *in vivo* tissues and organs. *In vivo* results of mouse tumor models further confirmed that MnO<sub>2</sub>-PDA@Lipo@Geb@Beb nano-drug could effectively inhibit the growth of NSCLC cells. Therefore, it was proved that the combination of MnO<sub>2</sub>, liposomes, Geb, and Beb could effectively induce the apoptosis of lung cancer cells and inhibit the development of NSCLC by integrating their respective advantages.

#### 4. Discussion

In conclusion, this study reported a novel pH-responsive MnO<sub>2</sub>-PDA@Lipo-coated Geb and Beb nanocomposite system as an inhibitor of NSCLC. The sensitive response of MnO<sub>2</sub> nanorods to acidic tumor microenvironment was the key factor for the effective release of anti-cancer drugs and tumor

growth inhibition through MnO<sub>2</sub>-PDA@Lipo@Geb@Beb nanocomposite system. The composite nano-material could guarantee (1) sustained release property of anti-cancer drug for effective treatment, (2) certain biological safety to reduce toxicity *in vivo*, and (3) effective combination of multidrug therapy. In this study, biodegradable and pH/GSH-responsive nanocomposite drug was designed to investigate its effects on the activity and apoptosis of lung cancer A549 cells and normal bronchial epithelial 16HBE cells, as well as the tumor progression. Meanwhile, we also systematically studied the inhibitory behavior of Geb, MnO<sub>2</sub>-PDA@Lipo@Geb, and MnO<sub>2</sub>-PDA@Lipo@Geb@Beb on NSCLC. Finally, the results of *in vitro* and *in vivo* experiments proved that the nanocomposite system successfully combined the advantages of MnO<sub>2</sub>, liposomes, Geb, and Beb, which could effectively inhibit the growth of NSCLC and maintain good biocompatibility. Therefore, it follows that MnO<sub>2</sub>-PDA@Lipo@Geb@Beb has great application potential in the nano-tumor medical engineering.

#### Acknowledgements

*Ethics approval:* This article contains the study with animal subjects.

#### Disclosure statement

The authors declare that they have no potential conflicts of interest.

## Funding

The author(s) reported there is no funding associated with the work featured in this article.

## Data availability statement

The data and materials in the current study are available from the corresponding author on reasonable request.

## References

- Alizadeh AA, Aranda V, Bardelli A, et al. (2015). Toward understanding and exploiting tumor heterogeneity. *Nat Med* 21:846–53.
- Allen TM, Cullis PR. (2013). Liposomal drug delivery systems: from concept to clinical applications. *Adv Drug Deliv Rev* 65:36–48.
- Barenholz Y. (2003). Relevancy of drug loading to liposomal formulation therapeutic efficacy. *J Liposome Res* 13:1–8.
- Chen H, Chen Z, Kuang Y, et al. (2018). Stepwise-acid-active organic/inorganic hybrid drug delivery system for cancer therapy. *Colloids Surf B Biointerfaces* 167:407–14.
- Chen LJ, Yang CX, Yan XP. (2017). Liposome-coated persistent luminescence nanoparticles as luminescence trackable drug carrier for chemotherapy. *Anal Chem* 89:6936–9.
- Drummond DC, Meyer O, Hong K, et al. (1999). Optimizing liposomes for delivery of chemotherapeutic agents to solid tumors. *Pharmacol Rev* 51:691–743.
- Ghosh K, Yue CY, Sk MM, Jena RK. (2017). Development of 3D urchin-shaped coaxial manganese dioxide@polyaniline (MnO<sub>2</sub>@PANI) composite and self-assembled 3D pillared graphene foam for asymmetric all-solid-state flexible supercapacitor application. *ACS Appl Mater Interfaces* 9:15350–63.
- Han Y, Li Y, Zhang P, et al. (2016). Nanostructured lipid carriers as novel drug delivery system for lung cancer gene therapy. *Pharm Dev Technol* 21:277–81.
- He Q, Chen J, Yan J, et al. (2020). Tumor microenvironment responsive drug delivery systems. *Asian J Pharm Sci* 15:416–48.
- Jin H, Wan C, Zou Z, et al. (2018). Tumor ablation and therapeutic immunity induction by an injectable peptide hydrogel. *ACS Nano* 12:3295–310.
- Lasic DD, Frederik PM, Stuart MC, et al. (1992). Gelation of liposome interior. A novel method for drug encapsulation. *FEBS Lett* 312:255–8.
- Li B, Rong G, Xie Y, et al. (2006). Low-temperature synthesis of alpha-MnO<sub>2</sub> hollow urchins and their application in rechargeable Li batteries<sup>+</sup>. *Inorg Chem* 45:6404–10.
- Liao L, Liu J, Dreaden EC, et al. (2014). A convergent synthetic platform for single-nanoparticle combination cancer therapy: ratiometric loading and controlled release of cisplatin, doxorubicin, and camptothecin. *J Am Chem Soc* 136:5896–9.
- Liu D, Liu F, Liu Z, et al. (2011). Tumor specific delivery and therapy by double-targeted nanostructured lipid carriers with anti-VEGFR-2 antibody. *Mol Pharm* 8:2291–301.
- Liu G, Ma J, Li Y, et al. (2017). Core-interlayer-shell Fe<sub>3</sub>O<sub>4</sub>@mSiO<sub>2</sub>@lipid-PEG-methotrexate nanoparticle for multimodal imaging and multi-stage targeted chemo-photodynamic therapy. *Int J Pharm* 521:19–32.
- Liu Y, Chen XG, Yang PP, et al. (2019). Tumor microenvironmental pH and enzyme dual responsive polymer-liposomes for synergistic treatment of cancer immuno-chemotherapy. *Biomacromolecules* 20:882–92.
- Lohcharenkal W, Wang L, Chen YC, Rojanasakul Y. (2014). Protein nanoparticles as drug delivery carriers for cancer therapy. *Biomed Res Int* 2014:180549.
- Lusic H, Grinstaff MW. (2013). X-ray-computed tomography contrast agents. *Chem Rev* 113:1641–66.
- Maeda H, Wu J, Sawa T, et al. (2000). Tumor vascular permeability and the EPR effect in macromolecular therapeutics: a review. *J Control Release* 65:271–84.
- Papahadjopoulos D, Allen TM, Gabizon A, et al. (1991). Sterically stabilized liposomes: improvements in pharmacokinetics and antitumor therapeutic efficacy. *Proc Natl Acad Sci U S A* 88:11460–4.
- Prasad R, Chauhan DS, Yadav AS, et al. (2018). A biodegradable fluorescent nanohybrid for photo-driven tumor diagnosis and tumor growth inhibition. *Nanoscale* 10:19082–91.
- Prasad R, Yadav AS, Gorain M, et al. (2019). Graphene oxide supported liposomes as red emissive theranostics for phototriggered tissue visualization and tumor regression. *ACS Appl Bio Mater* 2:3312–20.
- Qu Q, Zhang P, Wang B, et al. (2009). Electrochemical performance of MnO<sub>2</sub> nanorods in neutral aqueous electrolytes as a cathode for asymmetric supercapacitors. *J Phys Chem C* 113:14020–7.
- Selvakumar M, Srivastava P, Pawar HS, et al. (2016). On-demand guided bone regeneration with microbial protection of ornamented SPU scaffold with bismuth-doped single crystalline hydroxyapatite: augmentation and cartilage formation. *ACS Appl Mater Interfaces* 8:4086–100.
- Wicki A, Witzigmann D, Balasubramanian V, Huwyler J. (2015). Nanomedicine in cancer therapy: challenges, opportunities, and clinical applications. *J Control Release* 200:138–57.
- Wu M-X, Yan H-J, Gao J, et al. (2018). Multifunctional supramolecular materials constructed from polypyrrole@UiO-66 nanohybrids and pillararene nanovalves for targeted chemophotothermal therapy. *ACS Appl Mater Interfaces* 10:34655–63.
- Yanasarn N, Sloat BR, Cui Z. (2011). Negatively charged liposomes show potent adjuvant activity when simply admixed with protein antigens. *Mol Pharm* 8:1174–85.
- Yang G, Xu L, Chao Y, et al. (2017). Hollow MnO<sub>2</sub> as a tumor-microenvironment-responsive biodegradable nano-platform for combination therapy favoring antitumor immune responses. *Nat Commun* 8:902.
- Ying M, Zhan C, Wang S, et al. (2016). Liposome-based systemic glioma-targeted drug delivery enabled by all-d peptides. *ACS Appl Mater Interfaces* 8:29977–85.
- Zamboni WC. (2005). Liposomal, nanoparticle, and conjugated formulations of anticancer agents. *Clin Cancer Res* 11:8230–4.
- Zhang F, Chen D, Wang Y, et al. (2017). Lysosome-dependent necrosis specifically evoked in cancer cells by gold nanorods. *Nanomedicine* 12:1575–89.
- Zhang JL, Srivastava RS, Misra RD. (2007). Core-shell magnetite nanoparticles surface encapsulated with smart stimuli-responsive polymer: synthesis, characterization, and LCST of viable drug-targeting delivery system. *Langmuir* 23:6342–51.
- Zhang T, Zhou W, Jia Z, et al. (2018). Polydopamine-assisted functionalization of heparin and vancomycin onto microarc-oxidized 3D printed porous Ti6Al4V for improved hemocompatibility, osteogenic and anti-infection potencies. *Sci China Mater* 61:579.
- Zhang Y, Wu L, Jiang C, Yan B. (2015). Reprogramming cellular signaling machinery using surface-modified carbon nanotubes. *Chem Res Toxicol* 28:296–305.
- Zhu S, Chen Z, Wang L, et al. (2018). A combination of SAHA and quina-crone is effective in inducing cancer cell death in upper gastrointestinal cancers. *Clin Cancer Res* 24:1905–16.
- Zununi Vahed S, Salehi R, Davaran S, Sharifi S. (2017). Liposome-based drug co-delivery systems in cancer cells. *Mater Sci Eng C Mater Biol Appl* 71:1327–41.